

Spatial order in a two-dimensional spin-orbit-coupled spin-1/2 condensate: superlattice, multi-ring and stripe formation

S. K. Adhikari*

Instituto de Física Teórica, Universidade Estadual Paulista - UNESP, 01.140-070 São Paulo, São Paulo, Brazil

(Dated: August 2, 2021)

We demonstrate the formation of stable spatially-ordered states in a *uniform* and also *trapped* quasi-two-dimensional (quasi-2D) Rashba or Dresselhaus spin-orbit (SO) coupled pseudo spin-1/2 Bose-Einstein condensate using the mean-field Gross-Pitaevskii equation. For weak SO coupling, one can have a circularly-symmetric $(0, +1)$ - or $(0, -1)$ -type multi-ring state with intrinsic vorticity, for Rashba or Dresselhaus SO coupling, respectively, where the numbers in the parentheses denote the net angular momentum projection in the two components, in addition to a circularly-asymmetric degenerate state with zero net angular momentum projection. For intermediate SO couplings, in addition to the above two types, one can also have states with stripe pattern in component densities with no periodic modulation in total density. The stripe state continues to exist for large SO coupling. In addition, a new spatially-periodic state appears in the uniform system: a *superlattice* state, possessing some properties of a *supersolid*, with a square-lattice pattern in component densities and also in total density. In a trapped system the superlattice state is slightly different with multi-ring pattern in component density and a square-lattice pattern in total density. For an equal mixture of Rashba and Dresselhaus SO couplings, in both uniform and trapped systems, only stripe states are found for all strengths of SO couplings. In a uniform system all these states are quasi-2D solitonic states.

I. INTRODUCTION

The pursuit of a supersolid [1] has lately gained impetus among research workers in different areas of low-temperature physics. A supersolid is a special form of matter possessing the properties of both a crystalline solid and a superfluid. It is characterized by a spatially-ordered periodic matter resulting from a breakdown of continuous translational invariance as in a crystalline solid. It also enjoys a frictionless flow as in a superfluid, breaking continuous gauge invariance. Hence a supersolid is a special type of superfluid and its search has been confined to a superfluid, e.g., Bose-Einstein condensate (BEC) [2], and Fermi superfluid [3]. The search of a supersolid helium [4] was inconclusive [5]. Following theoretical suggestions to create a supersolid with finite-range [6] and dipolar [7] interactions, different experimental groups confirmed supersolidity in a quasi-one-dimensional (quasi-1D) [8] and a quasi-two-dimensional (quasi-2D) [9] dipolar trapped BEC.

There have been theoretical suggestions for creating supersolid-like states in a spin-orbit-coupled (SO-coupled) BEC [10]. Although there cannot be a natural spin-orbit (SO) coupling in a neutral atom, an artificial synthetic SO coupling is possible by tuned Raman lasers that couple the different spin component states [11] of a spinor BEC [12]. Two such possible SO couplings are due to Rashba [13] and Dresselhaus [14]. An equal mixture of these SO couplings has been experimentally realized in a pseudo spin-1/2 ($F = 1/2$) ^{23}Na

[15] and ^{87}Rb [16] BEC of $F_z = 0, -1$ spin component states. A pseudo spin-1/2 state contains only the components $F_z = 0, -1$ of a hyperfine spin-1 ($F = 1$) state. The mean-field equation of this system is governed by the Pauli spin matrices and hence the name pseudo spin-1/2. Later, an SO-coupled spin-1 ^{87}Rb BEC of $F_z = \pm 1, 0$ spin component states was also realized [17]. Recently, a spatially-periodic supersolid-like state with stripe pattern in density, called a superstripe state, was observed in an SO-coupled quasi-1D pseudo spin-1/2 spinor BEC of ^{23}Na atoms [18] employing an equal mixture of Rashba and Dresselhaus couplings. There have been theoretical studies on the stability of different phases of BECs with Rashba-Dresselhaus spin-orbit coupling against quantum and thermal fluctuations [19].

In view of the observed superstripe state in an SO-coupled quasi-1D pseudo spin-1/2 spinor BEC [18], in this paper we look for a supersolid-like state [1] in a quasi-2D pseudo spin-1/2 SO-coupled spinor BEC using the mean-field Gross-Pitaevskii (GP) equation [20]. Previous considerations were limited to a stripe state in a quasi-1D pseudo spin-1/2 SO-coupled spinor BEC [21, 22]. In a quasi-2D trap, different types of spatially-ordered 2D lattice states seem likely in an SO-coupled pseudo spin-1/2 spinor BEC, specially after the confirmation of such states in an SO-coupled quasi-2D spin-1 spinor BEC [23, 24]. We will consider both uniform (trapless) and trapped states in this study under the action of Rashba or Dresselhaus SO coupling, in addition to an equal mixture of Rashba and Dresselhaus couplings.

First we will consider a uniform system, where the localized state appears in the form of a quasi-2D soliton. In a scalar BEC, solitons cannot be stabilized in two [25] and three dimensions [26] due to a collapse instability. However, a pseudo spin-1/2 SO-coupled BEC can sustain

*sk.adhikari@unesp.br

<https://professores.ift.unesp.br/sk.adhikari/>

a quasi-1D [27] or a quasi-2D [28] or a 3D [29] soliton. We identify a variety of solitons in an SO-coupled quasi-2D pseudo spin-1/2 spinor BEC. For a weak SO coupling there can be two types of degenerate solitonic states with very large spatial extension: circularly-symmetric $(0, \pm 1)$ -type multi-ring and circularly-asymmetric solitons, where the numbers in parenthesis indicate the angular momentum projection in the two components with the upper (lower) sign corresponding to Rashba (Dresselhaus) SO coupling. The $(0, \pm 1)$ -type multi-ring state has $1/2$ unit of total angular momentum projection and often is classified as a half-vortex state [30, 31]. Each component of the circularly-asymmetric soliton hosts an antivortex-vortex pair resulting in zero net angular momentum projection in each. With the increase of SO coupling, a stripe state with stripe pattern in component densities appears. For strong SO coupling two types of degenerate solitonic states appear: a state with stripe pattern in density without any modulation in total density and a superlattice state with square-lattice pattern in both component and total densities. The present solitons with a 2D square-lattice structure in total density [21], viz. figures 6(d)-(f), sharing properties with, and more closely related to, a conventional supersolid, will be termed superlattice solitons in the following as suggested in Refs. [21–24]. The multi-ring, viz. figures 5(a)-(c), and stripe solitons, viz. figures 6(a)-(c), only exhibit a spatially-periodic pattern in the component densities without any periodic pattern in the total density. Nevertheless, in the literature such a state with stripe pattern in component density only, also bearing some similarity to a supersolid, has often been termed a superstripe state [18, 21, 22]. In this paper we call such a state by the name stripe state to differentiate it from the superlattice state with square-lattice pattern in total density. For an equal mixture of Rashba and Dresselhaus SO couplings we find only stripe solitons for all values of SO couplings; these solitons have a stripe pattern in component densities with no spatially-periodic pattern in total density. To generate an equal mixture of Rashba and Dresselhaus couplings in a laboratory a pair of Raman lasers coupling the spin-component states are needed [16], whereas to create a Rashba or a Dresselhaus coupling multiple Raman laser beams are needed [32], which leads to a more complex electromagnetic “trapping” potential. Hence it seems reasonable that a Rashba or a Dresselhaus SO-coupled BEC may host different types of superlattice states not possible in the case of an equal mixture of Rashba and Dresselhaus couplings.

The scenario of spatially-ordered states in a harmonically-trapped SO-coupled quasi-2D pseudo spin-1/2 BEC remains almost the same when compared with a uniform system. For a weak SO coupling, the trapped system can host three types of states: circularly-symmetric $(0, \pm 1)$ -type multi-ring state, circularly-asymmetric state and stripe state. For large SO coupling, one encounters two types of spatially-periodic states: stripe state and a special type of

multi-ring state. This multi-ring state possesses a multi-ring pattern in component density with a square-lattice pattern in total density near the center thus exhibiting a supersolid-like behavior.

In section II A we present the mean-field GP equation that we use in this investigation. In section II B we demonstrate the plausibility of the appearance of the $(0, \pm 1)$ -type state, stripe state, and superlattice state from a consideration of linear version of this model. The numerical result is presented in section III. In section III A the results for a uniform quasi-2D pseudo spin-1/2 Rashba and Dresselhaus SO-coupled self-attractive BEC soliton are presented. Those for an equal mixture of Rashba and Dresselhaus couplings are presented in section III B. The results for a uniform quasi-2D pseudo spin-1/2 Rashba and Dresselhaus SO-coupled self-repulsive BEC soliton are presented in section III C. The results for a harmonically trapped SO-coupled quasi-2D BEC are presented in section III D. Finally, a summary of our findings is given in section IV.

II. MEAN-FIELD MODEL

A. Gross-Pitaevskii equation

We consider a BEC of N atoms, each of mass m , under a harmonic trap $V(\mathbf{r}) = m\omega^2(x^2 + y^2)/2 + m\omega_z^2 z^2/2$ ($\omega_z \gg \omega$) of frequency ω_z and ω in the z direction and in the $x - y$ plane, respectively. The single particle Hamiltonian of the SO-coupled BEC is [16]

$$H_0 = -\frac{\hbar^2}{2m}\nabla_{\mathbf{r}}^2 + V(\mathbf{r}) + \gamma[\eta p_y \sigma_x - p_x \sigma_y], \quad (1)$$

where $\mathbf{r} \equiv \{x, y, z\}$, $\nabla_{\mathbf{r}}^2 = (\partial^2/\partial x^2 + \partial^2/\partial y^2 + \partial^2/\partial z^2) \equiv (\partial_x^2 + \partial_y^2 + \partial_z^2)$, γ is the strength of the SO-coupling term in square bracket, $\eta = +1$ for Rashba coupling, $\eta = -1$ for Dresselhaus coupling, and $\eta = 0$ for an equal mixture of Rashba and Dresselhaus couplings, momentum component $p_x = -i\hbar\partial_x$, $p_y = -i\hbar\partial_y$ and the Pauli spin matrices σ_x and σ_y are

$$\sigma_x = \begin{pmatrix} 0 & 1 \\ 1 & 0 \end{pmatrix}, \quad \sigma_y = \begin{pmatrix} 0 & -i \\ i & 0 \end{pmatrix}. \quad (2)$$

Under a strong trap in the z direction, the system is assumed to be frozen in the Gaussian ground state in the z direction and the relevant dynamics in the $x - y$ plane, obtained by integrating out the z coordinate in a straight-forward fashion [33], leads to the following set of GP equations at zero temperature for spin components $F_z = 0, -1$ [34]

$$i\partial_t \psi_1(\boldsymbol{\rho}, t) = [H_{\boldsymbol{\rho}} + c_0 n_1(\boldsymbol{\rho}, t) + c_2 n_2(\boldsymbol{\rho}, t)] \psi_1(\boldsymbol{\rho}, t) + \gamma(-i\eta\partial_y + \partial_x)\psi_2(\boldsymbol{\rho}, t), \quad (3)$$

$$i\partial_t \psi_2(\boldsymbol{\rho}, t) = [H_{\boldsymbol{\rho}} + c_0 n_2(\boldsymbol{\rho}, t) + c_2 n_1(\boldsymbol{\rho}, t)] \psi_2(\boldsymbol{\rho}, t) - \gamma(i\eta\partial_y + \partial_x)\psi_1(\boldsymbol{\rho}, t), \quad (4)$$

$$H_\rho = -\frac{1}{2}\nabla_\rho^2 + \frac{1}{2}\rho^2, \quad (5)$$

$$c_0 = N\sqrt{2\pi\kappa a_0}, \quad c_2 = N\sqrt{2\pi\kappa a_{12}}, \quad (6)$$

where $\rho = \{x, y\}$, $\kappa = \omega_z/\omega$, $\partial_t \equiv \partial/\partial t$, $\nabla_\rho^2 = \partial_x^2 + \partial_y^2$, $n_j = |\psi_j|^2$, $j = 1, 2$ are the densities of spin components $F_z = 0, -1$, and $n(\rho) = \sum_j n_j(\rho)$ the total density, a_0 (a_2) is the intraspecies (interspecies) scattering length. All quantities in (3)-(4) and in the following are dimensionless; this is achieved by expressing length in units of oscillator length $l_0 \equiv \sqrt{\hbar/m\omega}$, density in units of l_0^{-2} , energy in units of $\hbar\omega$, and time in units of ω^{-1} . The normalization condition is $\int n(x, y) dx dy = 1$.

The time-independent version of (3)-(4), appropriate for stationary solutions, can be derived from the energy functional

$$E[\psi] = \int dx dy \left\{ \sum_j \frac{1}{2} |\nabla_\rho \psi_j|^2 + \frac{1}{2} c_0 (n_1^2 + n_2^2) + c_2 n_1 n_2 + \frac{1}{2} \rho^2 n + \gamma [\psi_1^* (\partial_x - i\eta \partial_y) \psi_2 - \psi_2^* (\partial_x + i\eta \partial_y) \psi_1] \right\}. \quad (7)$$

Equations (3), (4), and (7) are valid for a harmonically trapped quasi-2D SO-coupled pseudo spin-1/2 spinor BEC. The same for a uniform system can be obtained by taking the limit $\omega \rightarrow 0$ and removing the harmonic trap from these equations. For a uniform system (3) and (4) remain valid with

$$c_0 = N\sqrt{2\pi}a_0, \quad c_2 = N\sqrt{2\pi}a_{12}. \quad (8)$$

Now length is expressed in units of $l_z = \sqrt{\hbar/m\omega_z}$, density in units of l_z^{-2} , and energy in units of $\hbar\omega_z$, and time in units of ω_z^{-1} .

B. Analytic Consideration

Many properties of the density distribution can be understood from a consideration of the single-particle Hamiltonian in the absence of nonlinear interaction. First we consider a Rashba or a Dresselhaus SO coupling. The quasi-2D wave function of the single-particle Hamiltonian

$$H_0^{2D} = -\frac{1}{2}\nabla_\rho^2 - i\gamma[\eta\partial_y\sigma_x - \partial_x\sigma_y] \quad (9)$$

satisfies the following eigenvalue equation

$$\begin{bmatrix} -\frac{1}{2}\nabla_\rho^2 & \gamma(\partial_x - i\eta\partial_y) \\ -\gamma(\partial_x + i\eta\partial_y) & -\frac{1}{2}\nabla_\rho^2 \end{bmatrix} \begin{pmatrix} \psi_1 \\ \psi_2 \end{pmatrix} = \mathcal{E} \begin{pmatrix} \psi_1 \\ \psi_2 \end{pmatrix}, \quad (10)$$

with energy \mathcal{E} . In circular coordinates $\rho = \{\rho, \theta\}$, $x = \rho \cos \theta$, $y = \rho \sin \theta$, we have $(\partial_x \pm i\partial_y) = \exp(\pm i\theta)(\partial_\rho \pm i\partial_\theta/\rho)$, with $\partial_\rho \equiv \partial/\partial\rho$, $\partial_\theta \equiv \partial/\partial\theta$. A circularly-symmetric solution of angular momentum projection m of (10) will have the form [31]

$$\psi_m(\rho) = \begin{pmatrix} \psi_1(\rho) \\ \psi_2(\rho) \exp(i\eta\theta) \end{pmatrix} \frac{\exp(im\theta)}{\sqrt{2\pi}}. \quad (11)$$

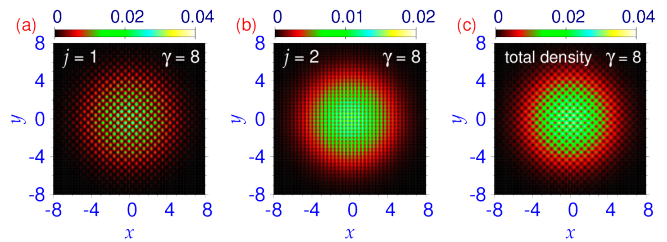


FIG. 1: Contour plot of density n_j of the state (15) for $\gamma = 8$ and $\eta = 1$ of components (a) $j = 1$ (n_1), (b) $j = 2$ (n_2) and (c) total density after multiplying the state (15) by an appropriate Gaussian distribution. The densities are normalized as $\int dx dy n(x, y) = 1$. Results in all figures are plotted in dimensionless units.

As $\eta = \pm 1$ for Rashba and Dresselhaus SO couplings, respectively, we find that the second component carries a relative angular momentum projection η with respect to the first component in addition to a possible overall angular momentum projection m . All states with $|m| > 1$ are unstable in general, hence a stable state of type (11) is a state of type $(0, \eta)$ or $(0, \pm 1)$ for Rashba or Dresselhaus SO coupling. Considering $m = \mp 1$, we can have an equivalent state of type $(\mp 1, 0)$. These two types are all states with angular momentum projection less than unity. Of these two types of equivalent states $-(0, \pm 1)$ and $(\mp 1, 0)$, in this study we consider only the state of type $(0, \pm 1)$. This state has angular momentum projection $m = 0$ and spin $s = 1/2$, hence the total angular momentum projection $j_z = m + s_z = 1/2$ and this state is often called a quantum half-vortex state.

The appearance of the stripe state can be understood from the consideration that (10) has the following degenerate solutions

$$\begin{pmatrix} \psi_1 \\ \psi_2 \end{pmatrix} = \begin{pmatrix} \cos(\gamma x) \\ -\sin(\gamma x) \end{pmatrix}, \quad (12)$$

$$\begin{pmatrix} \psi_1 \\ \psi_2 \end{pmatrix} = \begin{pmatrix} \cos(\gamma y) \\ -i\eta \sin(\gamma y) \end{pmatrix}, \quad (13)$$

with energy

$$\mathcal{E} = -\frac{\gamma^2}{2}. \quad (14)$$

The solutions (12) and (13) represent stripes along y and x directions, respectively. There is another set of equivalent solutions which we will not consider: $(\psi_1, \psi_2)^T = (\sin(\gamma x), \cos(\gamma x))^T$ and $(\psi_1, \psi_2)^T = (\sin(\gamma y), i\eta \cos(\gamma y))^T$; these states represent stripes in density along x and y directions in the components. Both sets of solutions have uniform density in the sum of the two components: $|\psi_1|^2 + |\psi_2|^2 = 1$.

A linear combination of the degenerate states (12) and (13), e.g.

$$\begin{pmatrix} \psi_1 \\ \psi_2 \end{pmatrix} = \sqrt{n} \begin{pmatrix} \cos(\gamma x) \pm \cos(\gamma y) \\ -\sin(\gamma x) \mp i\eta \sin(\gamma y) \end{pmatrix}, \quad (15)$$

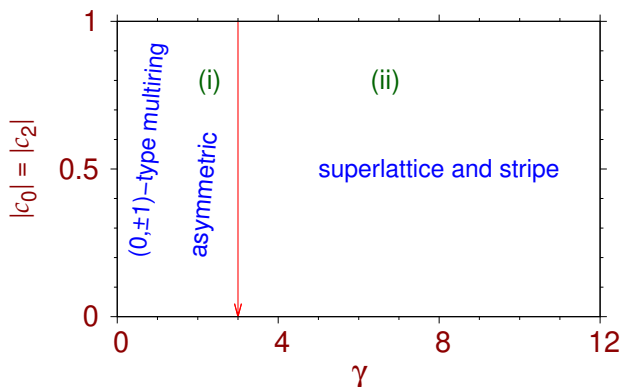


FIG. 2: The $c_0 = c_2$ versus γ phase plot showing soliton formation in a Rashba or a Dresselhaus SO-coupled pseudo spin-1/2 BEC in different regions of parameter space: (i) formation of circularly-symmetric $(0, \pm 1)$ -type multi-ring and circularly-asymmetric solitons and (ii) superlattice and stripe solitons.

is also a valid eigenfunction and represents a square-lattice pattern in density of the components as well as in the total density. The spatial modulation in density is produced by the sin and cos terms in (15).

It is tempting to multiply the functions (12), (13), and (15) by a localized Gaussian distribution and see if such a state can simulate the density of a localized stripe or superlattice state. The answer is affirmative. The density pattern of the state (12) or (13) after this multiplication is quite similar to the density of a localized stripe state (result not shown here) obtained by a numerical solution of the GP equation. The total density of the stripe state does not have any spatially-periodic modulation. In figure 1, we display a contour plot of the density of components (a) $j = 1$, (b) $j = 2$, and (c) total density of the state (15) for $\gamma = 8, \eta = +1$ after multiplying by an appropriate Gaussian. The density of this state is quite similar to a superlattice soliton with square-lattice pattern in density for $\gamma = 8, c_0 = c_2 = -0.5$, viz. figures 6(d)-(f). Even the total density in figure 1(c) has a square-lattice pattern as in a superlattice BEC. Hence an analytic consideration of the single-particle Hamiltonian (9) reveals that it can naturally lead to eigenstates with densities in agreement with those in an actual physical $(0, \pm 1)$ -type state, stripe state and superlattice state in a SO-coupled spin-1/2 BEC. In a weakly-attractive uniform system, that we consider in this paper, the energies of these states are very close to the analytic energy $\mathcal{E} = -\gamma^2/2$ in most cases, indicating a negligible contribution from the nonlinear terms c_0 and c_2 .

For an equal mixture of Rashba and Dresselhaus SO couplings ($i\gamma\partial_x\sigma_y$), (10) becomes

$$\begin{bmatrix} -\frac{1}{2}\nabla_{\rho}^2 & \gamma\partial_x \\ -\gamma\partial_x & -\frac{1}{2}\nabla_{\rho}^2 \end{bmatrix} \begin{pmatrix} \psi_1 \\ \psi_2 \end{pmatrix} = \mathcal{E} \begin{pmatrix} \psi_1 \\ \psi_2 \end{pmatrix}. \quad (16)$$

Equation (16) does not allow $(0, \pm 1)$ -type state implied by (11). Equation (16) has the spatially-periodic stripe solution (12). This solution $(\cos(\gamma x), -\sin(\gamma x))^T$ with

energy $\mathcal{E} = -\gamma^2/2$ represents stripe in density along y direction. There is no degenerate solution, similar to (13), with the same energy. Thus there can be no solution of type (15) in this case, which could represent a superlattice state with square-lattice pattern in density.

III. NUMERICAL RESULT

To solve (3) and (4) numerically, we propagate these in time by the split-time-step Crank-Nicolson discretization scheme [35] using a space step of $dx = dy = 0.05$ and a time step of $dt = dx^2 \times 0.1$ for imaginary-time propagation and a time step of $dt = dx^2 \times 0.05$ for real-time propagation. In all calculations of stationary states, we employ imaginary-time approach with the conservation of normalization ($= \int dx dy [n_1(x, y) + n_2(x, y)]$) during time propagation, which finds the lowest-energy solution of each type. Real-time propagation is used to test the stability of the solitons. The quantity ($M = \int dx dy [n_1(x, y) - n_2(x, y)]$) is not a good quantum number and is left to freely evolve during time propagation to attain a final converged value consistent with the parameters of the problem. The converged value of the quantity M was found to be essentially zero in all untrapped cases, viz. figures 3-8, indicating an equal number of atoms in the two components. The same could have a small nonzero value ($\lesssim 0.1$) for the trapped case for small values of γ , viz. figure 9(a)-(f).

A. Uniform SO-coupled quasi-2D spin-1/2 BEC: Rashba/Dresselhaus coupling

We study the formation of a spatially-ordered periodic pattern in density of a self-attractive ($c_0 < 0$) quasi-2D SO-coupled uniform pseudo spin-1/2 BEC for different sets of parameters: the nonlinearities c_0, c_2 and SO-coupling strength γ . Without losing generality we will consider only the case $c_2 < 0$ with $c_0 = c_2$. The scenario of soliton formation for Rashba or Dresselhaus SO coupling is illustrated in the phase plot of $c_0 = c_2$ versus γ for $c_2 < 0$ in figure 2 for small values of c_0 ($-1 < c_0 < 0$). Circularly-symmetric $(0, \pm 1)$ -type multi-ring solitons and circularly-asymmetric solitons are formed in region (i), superlattice and stripe solitons are formed in region (ii).

First, we consider a $(0, \pm 1)$ -type multi-ring soliton for a small γ ($\gamma = 0.5$) for Rashba (upper sign) or Dresselhaus (lower sign) SO coupling. In figure 3 we display the contour plot of density of the central region of components (a) $j = 1$, (b) $j = 2$, and (c) total density of a $(0, \pm 1)$ -type multi-ring soliton. In figures 4(a)-(b) we display the contour plot of the phase of wave function components $j = 1, 2$ of the circularly-symmetric $(0, +1)$ -type Rashba SO-coupled soliton of figures 3(a)-(c). In figure 4(b) there is a phase drop of $+2\pi$ under a complete rotation, indicating an angular momentum projection of

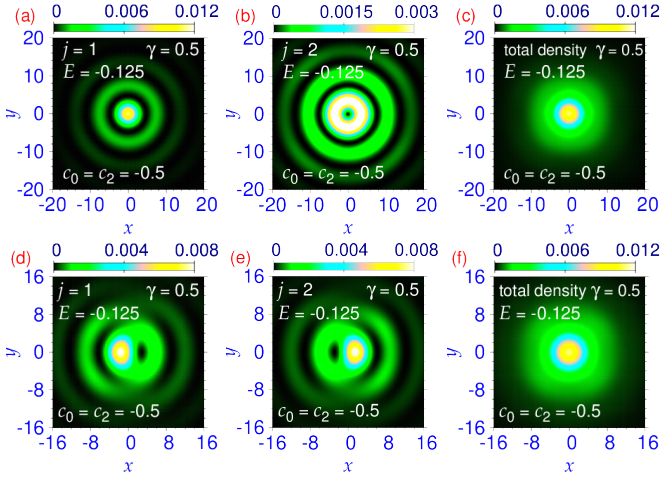


FIG. 3: Contour plot of density n_j of a circularly-symmetric $(0, \pm 1)$ -type spin-1/2 Rashba or Dresselhaus SO-coupled BEC soliton for components (a) $j = 1$ (n_1), (b) $j = 2$ (n_2) and (c) total density (n); the same of a circularly-asymmetric spin-1/2 Rashba or Dresselhaus SO-coupled BEC soliton with an antivortex-vortex structure in each component for (d) $j = 1$, (e) $j = 2$ and (f) total density. The parameters are $c_0 = c_2 = -0.5$, $\gamma = 0.5$.

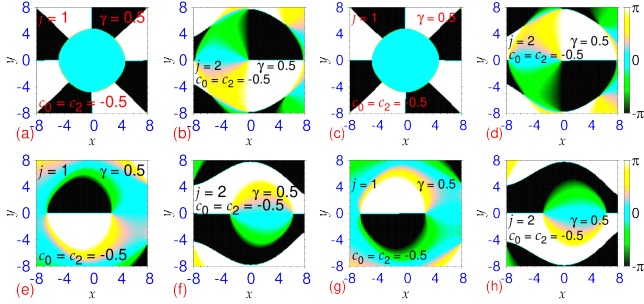


FIG. 4: Contour plot of phase of components (a) $j = 1$, and (b) $j = 2$ of the quasi-2D soliton of figures 2(a)-(b) for Rashba SO coupling, and (c)-(d) the same for Dresselhaus SO coupling; contour plot of phase of components (e) $j = 1$, and (f) $j = 2$ of the quasi-2D soliton of figures 2(d)-(e) for Rashba SO coupling, and (g)-(h) the same for Dresselhaus SO coupling.

+1 in component $j = 2$. There is no such phase drop in component $j = 1$. Although the densities of Rashba and Dresselhaus SO-coupled solitons are the same, the corresponding phases for Dresselhaus SO-coupling are different, viz. figures 4(c)-(d) showing the phases of components $j = 1, 2$ of the Dresselhaus SO-coupled soliton. In this case in figure 4(d) we find a phase drop of -2π under a complete rotation, indicating an angular momentum projection of -1 in this component. The contour plot of density of components (a) $j = 1$, (b) $j = 2$, and (c) total density of a circularly-asymmetric soliton is shown in figures 3(d)-(f) for Rashba or Dresselhaus SO coupling. Again the phases of the two SO couplings are different. In figures 4(e)-(f) we plot the phase of

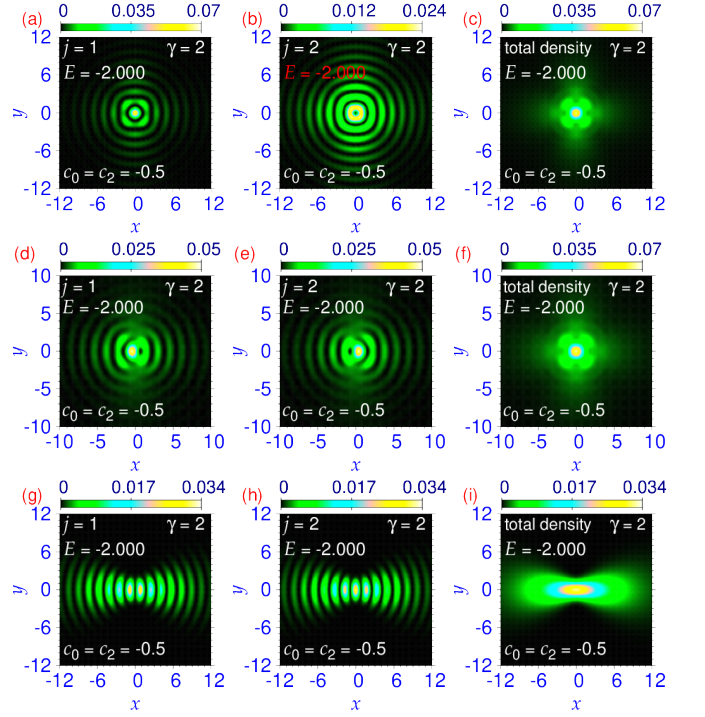


FIG. 5: Contour plot of density n_j of a circularly-symmetric $(0, \pm 1)$ -type spin-1/2 multi-ring Rashba or Dresselhaus SO-coupled BEC soliton for components (a) $j = 1$ (n_1), (b) $j = 2$ (n_2) and (c) total density (n); the same of a circularly-asymmetric spin-1/2 Rashba or Dresselhaus SO-coupled BEC soliton with an antivortex-vortex structure in each component for (d) $j = 1$, (e) $j = 2$ and (f) total density; the same of a spin-1/2 Rashba or Dresselhaus SO-coupled stripe soliton for (g) $j = 1$, (h) $j = 2$ and (i) total density. The parameters used are $c_0 = c_2 = -0.5$, $\gamma = 2$.

components $j = 1, 2$ of the wave function of the soliton of figures 3(d)-(e) for Rashba coupling, the same for Dresselhaus coupling are shown in figures 4(g)-(h). In all cases we find an antivortex-vortex pair of angular momentum projection -1 and $+1$ at two different places such that the net angular momentum projection in each component is zero. Of the vortex-antivortex pair, one is coreless [36]. In imaginary-time propagation, to obtain a $(0, \pm 1)$ -type multi-ring soliton, the appropriate vortex (antivortex) for Rashba (Dresselhaus) SO coupling in component $j = 2$ was imprinted in an initial Gaussian function as $\psi_2^{\text{initial}}(x, y) = (x \pm iy) \times \phi_{\text{Gauss}}(x, y)$. To obtain the circularly-asymmetric soliton, the initial wave function was taken to be a localized Gaussian function in the two components. The numerical energy of both types of degenerate solitons in figure 3 is $E = -0.125$, in agreement with the analytic result $\mathcal{E} = -\gamma^2/2 = -0.125$, viz. (14), independent of the type of SO coupling: Rashba or Dresselhaus.

To study multi-ring solitons for medium values of SO coupling ($\gamma = 2$), in figure 5 we show the contour plot of density of components (a) $j = 1$, (b) $j = 2$ and (c) total density of a circularly-symmetric $(0, \pm 1)$ -type multi-

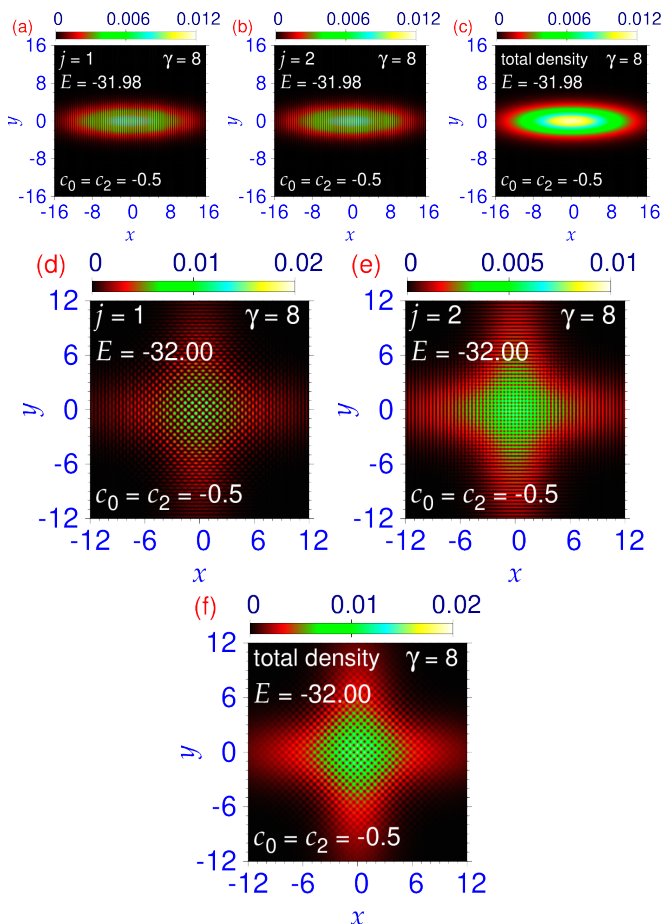


FIG. 6: Contour plot of density n_j of a pseudo spin-1/2 Rashba or Dresselhaus SO-coupled stripe soliton of components (a) $j = 1$ and (b) $j = 2$ (c) and total density. The same of a superlattice soliton of components (d) $j = 1$, (e) $j = 2$, and (f) the total density. The parameters used are $c_0 = c_2 = -0.5, \gamma = 8$.

ring soliton for Rashba or Dresselhaus SO coupling for $c_0 = c_2 = -0.5$. Although, there is a multi-ring structure in density of the two components, the total density shows no spatially-periodic modulation. Multi-ring solitons were also investigated in a quasi-2D pseudo spin-1/2 SO-coupled BEC trapped in a radially periodic potential [37] which creates a multi-ring modulation in density. However, the present radial modulation in density without any external trap is a consequence of the SO coupling. The increase of γ from figures 3(a)-(c) to figures 5(a)-(c) has increased the binding, and hence aids in forming the compact solitons. In figures 5(d)-(f) we display the circularly-asymmetric solitons for $c_0 = c_2 = -0.5, \gamma = 2$. These solitons are more compact and have developed asymmetric rings with the increase of γ from figures 3(d)-(f) to figures 5(d)-(f). In addition to these two types of solitons we find a new type of soliton not possible for a small SO coupling ($\gamma = 0.5$). These are the stripe solitons displayed in figures 5(g)-(i). To obtain these solitons the stripe pattern is imprinted on the initial wave function

as: $\psi_1^{\text{initial}}(x, y) \sim \sin(\gamma x) \times \phi_{\text{Gauss}}(x, y); \psi_2^{\text{initial}}(x, y) \sim \cos(\gamma x) \times \phi_{\text{Gauss}}(x, y)$. In this case the total density has no spatially-periodic modulation. The numerical energies of these three types of states for both Rashba and Dresselhaus SO couplings are identical ($E = -2.000$) and equal to the analytic energy of (14) ($\mathcal{E} = -\gamma^2/2 = -2$); hence these states can be considered degenerate.

As γ is increased, the $(0, \pm 1)$ -type multi-ring soliton ceases to exist and gives rise to a new type of soliton: superlattice soliton with square-lattice modulation in density. The stripe soliton and the circularly-asymmetric soliton continue to exist. However, as we are interested in spatially-periodic states, we will not consider the circularly-asymmetric soliton here. The spatial period of the lattice or stripe increases as γ is reduced. For a small γ , the size of the soliton is smaller than this period and the periodic pattern in density is not possible, viz figure 3 for $\gamma = 0.5$. In figure 6 we show a quasi-2D stripe soliton for $c_0 = c_2 = -0.5$, and $\gamma = 8$ through a contour plot of density of components (a) $j = 1$, (b) $j = 2$, and (c) total density, obtained by imaginary-time propagation using an initial localized wave function modulated by appropriate stripes in $j = 1$ and $j = 2$ components. Although, there is a stripe pattern in density in this case, the positions of maxima in component $j = 1$ coincide with the minima in component $j = 2$, thus resulting in a total density without modulation.

In figure 6 the superlattice soliton for the same set of parameters ($c_0 = c_2 = -0.5, \gamma = 8$) is displayed through a contour plot of density of components (d) $j = 1$, (e) $j = 2$, and (f) total density, obtained by imaginary-time propagation using the converged wave function of figures 5(a)-(c) as the initial state. The distribution of matter on a 2D square lattice is prominent in this case, not only in the component densities but also in the total density, viz. figure 6(f) [21]. The present superlattice soliton is a consequence of the SO coupling and breaks *continuous* translational symmetry as required in a supersolid [1]. The numerical density pattern of the components and the total density in this case are quite similar to the analytic component density and total density of figure 1. Again, for the same set of parameters, $c_0 = c_2 = -0.5, \gamma = 8$, the numerical energies of the stripe and superlattice solitons are the same ($E = -32.00$) and in agreement with the analytic estimate (14) ($\mathcal{E} = -\gamma^2/2 = -32$). Hence the spatially-periodic stripe and superlattice solitons can be considered to be degenerate.

B. Uniform SO-coupled quasi-2D spin-1/2 BEC: Equal-mixture coupling

Although the Rashba or Dresselhaus SO couplings are fundamental in nature, all experiments so far employed an equal mixture of Rashba and Dresselhaus SO couplings [15–17] ($-\gamma p_x \sigma_y$). This SO coupling is simpler in nature, involving partial derivative in one direction only, and is easily realizable in an experiment. Because

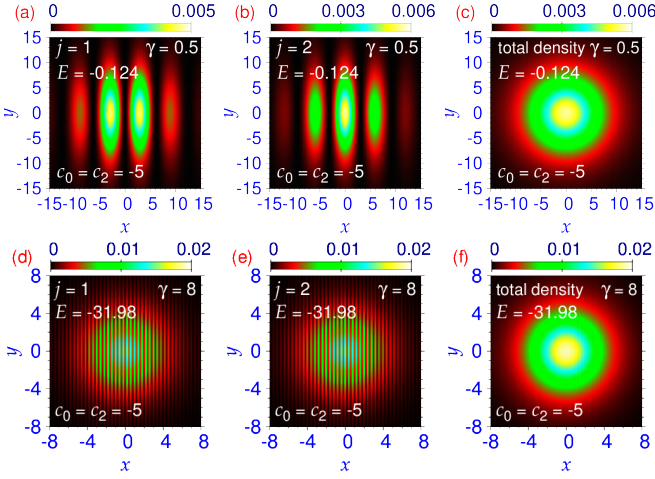


FIG. 7: Contour plot of density of a pseudo spin-1/2 stripe soliton for an equal mixture of Rashba and Dresselhaus couplings of components (a) $j = 1$, (b) $j = 2$ and (c) the total density for parameters $c_0 = c_2 = -5, \gamma = 0.5$. (d)-(f) The same densities for parameters $c_0 = c_2 = -5, \gamma = 8$.

of this phenomenological interest, we consider here the possibility of the formation of spatially-periodic pattern in a uniform quasi-2D pseudo spin-1/2 BEC under the action of an equal mixture of Rashba and Dresselhaus couplings. In this case, for all strengths of SO coupling γ , one can only have a soliton with a stripe pattern in component densities with a total density without such modulation. For a small γ ($=0.5$), the stripe soliton for $c_0 = c_2 = -5$ is displayed in figures 7(a)-(c), where we plot the density of components $j = 1, j = 2$, and the total density. In this case as the derivative SO coupling is of lower dimension acting only along the x direction, it has a weak localization capacity, hence we had to employ stronger attractive nonlinearity $c_0 = c_2 = -5$, in place of $c_0 = c_2 = -0.5$ used for Rashba or Dresselhaus coupling, to obtain a compact soliton. For large γ ($=8$), the stripe state for $c_0 = c_2 = -5$, and for an equal mixture of Rashba and Dresselhaus couplings, has a circular boundary as exhibited in figures 7(d)-(f) through a contour plot of densities of components $j = 1, j = 2$ and the total density. This boundary is elliptic for Rashba or Dresselhaus SO coupling in figures 6(a)-(c).

C. Uniform SO-coupled quasi-2D spin-1/2 self-repulsive BEC

So far we considered a uniform SO-coupled quasi-2D self-attractive BEC ($c_0 < 0$). It is also possible to have a self-repulsive ($c_0 > 0$) BEC. Such a self-repulsive BEC can be formed in a quasi-1D system [38], provided that the interspecies interaction is attractive. In the case of a uniform SO-coupled pseudo spin-1/2 BEC, the scenario of soliton formation of a self-repulsive BEC with attractive interspecies interaction is the same as a self-

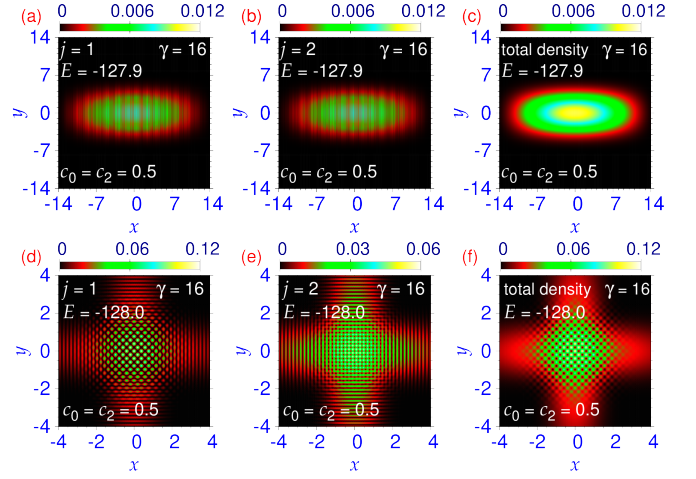


FIG. 8: Contour plot of density of a self-repulsive Rashba or Dresselhaus SO-coupled pseudo spin-1/2 stripe soliton of components (a) $j = 1$, (b) $j = 2$ and (c) the total density. The same of a superlattice soliton of components (d) $j = 1$, (e) $j = 2$ and (f) the total density. The parameters employed are $c_0 = c_2 = 0.5, \gamma = 16$.

attractive BEC. Nevertheless, due to SO coupling, one can also have a quasi-2D self-repulsive BEC soliton for repulsive interspecies interaction; such a soliton is not possible in the absence of SO coupling ($\gamma = 0$). Here we demonstrate the formation of a self-repulsive soliton in a Rashba or Dresselhaus SO-coupled quasi-2D pseudo spin-1/2 BEC for repulsive interspecies interaction. To this end we consider $c_0 = c_2 = 0.5$; these values of non-linearity lead to compact solitons of appropriate size for a not too small γ . In this case it is possible to have the same types of solitons as in the case of a self-attractive BEC for different strengths of SO coupling and we exhibit only the solitons for $\gamma = 16$ with pronounced spatially-periodic pattern in density. In figure 8, we display a contour plot of densities of an SO-coupled quasi-2D self-repulsive stripe BEC of components (a) $j = 1$, (b) $j = 2$ and (c) total density. The same of a superlattice BEC is shown in figures 8(d)-(f), where the square-lattice pattern in the total density is clearly visible. The numerical energies of the stripe and the superlattice solitons are $E = -127.9$ and -128.0 , respectively, in agreement with the analytic estimate (14) ($\mathcal{E} = -\gamma^2/2 = -128$).

D. Trapped SO-coupled quasi-2D BEC: Rashba/Dresselhaus coupling

We now investigate the formation of a spatially-ordered state in a trapped SO-coupled quasi-2D pseudo spin-1/2 BEC for Rashba or Dresselhaus coupling. The densities for Rashba or Dresselhaus SO couplings are the same for all sets of parameters. The scenario of the states for different strengths of SO coupling remain qualitatively the same as in the case of a uniform system. How-

ever, there are differences for large SO-coupling γ . In this case we consider a moderate value of nonlinearity $c_0 = c_2 = 100$. For a small γ , one can have a circularly-symmetric $(0, \pm 1)$ -type state; however, due to the harmonic trap it is not possible to have a multi-ring structure in the outer region as in the case of a uniform BEC for a small $\gamma \sim 1$. In figures 9(a)-(c) we display the contour plot of densities of the circularly-symmetric $(0, \pm 1)$ -type state for $\gamma = 1$. The same for the circularly-asymmetric state is quite similar to the densities in figures 3(d)-(f) (result not shown here). The densities of the stripe state for the same set of parameters are shown in figures 9(d)-(f). In this case, the circularly-symmetric $(0, \pm 1)$ -type state and the circularly-asymmetric state have the same energy $E = 3.375$, whereas the stripe state has a smaller energy $E = 3.363$. Hence the stripe state is the ground state. In fact, it is the ground state for all strengths of SO coupling. In the uniform case, considered so far, all these states, for a fixed γ , had approximately the same numerical energy and hence could be considered degenerate. The contour plot of densities of the stripe state for large strength of SO coupling $\gamma = 8$ and for $c_0 = c_2 = 100$ is shown in figures 9(g)-(i). For small values of nonlinearity c_0 and c_2 ($c_0, c_2 \lesssim 60$), the stripe state is the only possible stable state for large γ . For medium to large values of nonlinearity $c_0 = c_2 = 100$, one has a new type of excited multi-ring state with concentric ring pattern in the density of components $j = 1$ and $j = 2$ as displayed in figures 9(j)-(l); however, the total density has a square-lattice pattern in the central region and is without modulation in density in the outer region. However, the multi-ring state ($E = 27.99$) is an excited state compared to the stripe state ($E = 28.15$), which is the ground state. Nevertheless, the multi-ring state has supersolid-like properties. We also studied spatially-periodic states in a trapped SO-coupled quasi-2D spin-1/2 BEC for an equal mixture of Rashba and Dresselhaus couplings (result not presented in this paper). In that case only a stripe pattern can be obtained for all strengths of SO-coupling γ .

IV. SUMMARY AND DISCUSSION

To search for a supersolid-like spatially-ordered state in a uniform or harmonically-trapped pseudo spin-1/2 quasi-2D SO-coupled BEC, we find spatially periodic multi-ring, stripe, and superlattice states for large strengths of SO coupling γ . We consider Rashba and Dresselhaus SO couplings and an equal mixture of these couplings in this paper. For a small γ and for Rashba and Dresselhaus SO couplings, we could have two degenerate states: a circularly symmetric $(0, \pm 1)$ -type multi-ring state, and a circularly asymmetric state. For a large γ , the stripe state is obtained for all types of SO couplings in both uniform and trapped BECs. The stripe state has stripe pattern in component densities and no modulation in total density. The superlattice state is found only in

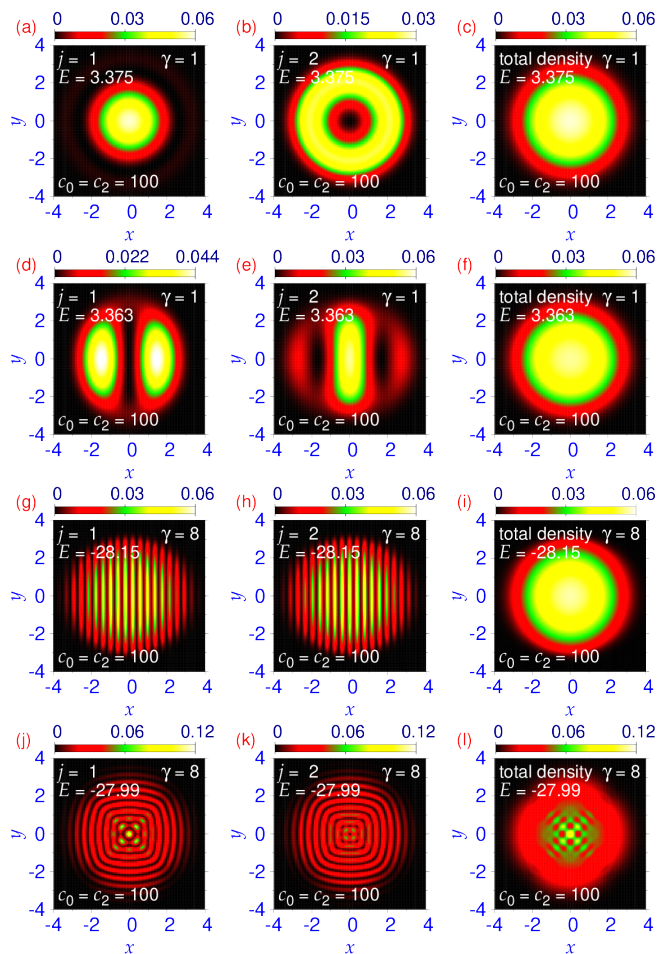


FIG. 9: Contour plot of density of a Rashba or Dresselhaus SO-coupled pseudo spin-1/2 harmonically-trapped circularly-symmetric $(0, \pm 1)$ -type BEC of components (a) $j = 1$, (b) $j = 2$ and (c) the total density for $\gamma = 1$. (d)-(f) The same densities of a stripe state. (g)-(i) The same densities of a stripe state for $\gamma = 8$. (j)-(l) The same densities of a multi-ring supersolid-like state for $\gamma = 8$. The nonlinearities are $c_0 = c_2 = 100$.

a uniform BEC for Rashba or Dresselhaus SO couplings and has a square-lattice pattern in component densities and also in total density, viz. figures 6(d)-(f) and 8(d)-(f). The multi-ring state is found in a uniform system for medium $\gamma (= 2)$, viz. figures 5(a)-(c), and in a trapped system for large $\gamma (= 8)$, viz. figures 9(m)-(o). In the case of a multi-ring state in a uniform system, there is no modulation in total density, whereas in the case of a trapped multi-ring state, there is a square-lattice modulation in the total density near the center indicating supersolid-like behavior. Nevertheless, the square-lattice pattern in the superlattice states in a uniform system is more prominent than the same in the trapped multi-ring state. In a uniform system, the stripe and the superlattice states have the same numerical energy and hence they are degenerate, whereas in a trapped system the stripe state is the ground state with lowest energy for all γ . For an equal

mixture of Rashba and Dresselhaus SO couplings, only a stripe state is obtained in all cases; for a small γ , no supersolid-like state is obtained. For a small γ , the solitonic states in a uniform SO-coupled BEC have very large spatial extension. All these states are dynamically stable, as we verified by real-time simulation over a long period of time as in the case of an SO-coupled spin-1 quasi-2D BEC [23, 24] (result not presented in this paper). Superlattice states were also found in an SO-coupled spin-1 spinor BEC [23]. However, it is more difficult to perform an experiment in an SO-coupled spin-1 spinor BEC with three spin components compared to an SO-coupled pseudo spin-1/2 spinor BEC with two spin components.

Hence we believe that the present study could motivate experiments in the search of superlattice states in an SO-coupled pseudo spin-1/2 spinor BEC. The superlattice soliton is dynamically robust and deserve further theoretical and experimental investigation.

Acknowledgments

The author acknowledges support by the CNPq (Brazil) grant 301324/2019-0, and by the ICTP-SAIFR-FAPESP (Brazil) grant 2016/01343-7

-
- [1] A. F. Andreev and I. M. Lifshitz, *Zurn. Eksp. Teor. Fiz.* 56, 2057 (1969) [English Transla.: *Sov. Phys. JETP* 29, 1107 (1969)]
A. J. Leggett, *Phys. Rev. Lett.* 25, 1543 (1970)
G. V. Chester, *Phys. Rev. A* 2, 256 (1970)
M. Boninsegni and N. V. Prokof'ev, *Rev. Mod. Phys.* 84, 759 (2012)
V. I. Yukalov, *Physics* 2, 49 (2020).
- [2] M. H. Anderson, J. R. Ensher, M. R. Matthews, C. E. Wieman, and E. A. Cornell, *Science* 269, 198 (1995)
K. B. Davis, M.-O. Mewes, M. R. Andrews, N. J. van Druten, D. S. Durfee, D. M. Kurn, and W. Ketterle, *Phys. Rev. Lett.* 75, 3969 (1995).
- [3] M. W. Zwierlein, C. H. Schunck, A. Schirotzek, and W. Ketterle, *Nature* 442, 54 (2006)
M. Greiner, C. A. Regal, and D. S. Jin, *Nature* 426, 537 (2003).
- [4] E. Kim and M. H. W. Chan, *Nature* 427, 225 (2004).
- [5] S. Balibar, *Nature* 464, 176 (2010).
- [6] G. Masella, A. Angelone, F. Mezzacapo, G. Pupillo, and N. V. Prokofev, *Phys. Rev. Lett.* 123, 045301 (2019)
F. Cinti, P. Jain, M. Boninsegni, A. Micheli, P. Zoller, and G. Pupillo, *Phys. Rev. Lett.* 105, 135301 (2010)
S. Sacconi, S. Moroni, and M. Boninsegni, *Phys. Rev. Lett.* 108, 175301 (2012).
- [7] R. Bombin, J. Boronat, F. Mazzanti, *Phys. Rev. Lett.* 119, 250402 (2017)
F. Cinti, M. Boninsegni, *J. Low Temp. Phys.* 196, 413 (2019)
Zhen-Kai Lu, Yun Li, D. S. Petrov, G. V. Shlyapnikov, *Phys. Rev. Lett.* 115 075303 (2015)
N. Y. Yao, C. R. Laumann, A. V. Gorshkov, S. D. Bennett, E. Demler, P. Zoller, M. D. Lukin, *Phys. Rev. Lett.* 109, 266804 (2012).
- [8] L. Tanzi, E. Lucioni, F. Famà, J. Catani, A. Fioretti, C. Gabbanini, R. N. Bisset, L. Santos, G. Modugno, *Phys. Rev. Lett.* 122, 130405 (2019)
G. Natale, R. M. W. van Bijnen, A. Patscheider, D. Pette, M. J. Mark, L. Chomaz, F. Ferlaino, *Phys. Rev. Lett.* 123, 050402 (2019).
- [9] F. Böttcher, J.-N. Schmidt, M. Wenzel, J. Hertkorn, M. Guo, T. Langen, T. Pfau, *Phys. Rev. X* 9, 011051 (2019)
J. Hertkorn, F. Böttcher, M. Guo, J. N. Schmidt, T. Langen, H. P. Büchler, T. Pfau, *Phys. Rev. Lett.* 123, 193002 (2019).
- [10] T.-L. Ho and S. Zhang, *Phys. Rev. Lett.* 107, 150403 (2011)
R. Liao, *Phys. Rev. Lett.* 120, 140403 (2018)
W. Han, X.-F. Zhang, D.-S. Wang, H.-F. Jiang, W. Zhang, and S.-G. Zhang, *Phys. Rev. Lett.* 121, 030404 (2018).
- [11] J. Dalibard, F. Gerbier, G. Juzeliūnas, P. Öhberg, *Rev. Mod. Phys.* 83, 1523 (2011)
V. Galitski and I. B. Spielman, *Nature* 494, 49 (2013).
- [12] J. Stenger, S. Inouye, D. M. Stamper-Kurn, H.-J. Miesner, A. P. Chikkatur, W. Ketterle, *Nature* 396, 345 (1998).
- [13] E. I. Rashba, *Fiz. Tverd. Tela* 2, 1224 (1960) [English Transla.: *Sov. Phys. Solid State* 2, 1109 (1960).]
- [14] G. Dresselhaus, *Phys. Rev.* 100, 580 (1955).
- [15] J. Li, W. Huang, B. Shteynas, S. Burchesky, F. C. Top, E. Su, J. Lee, A. O. Jamison, and W. Ketterle, *Phys. Rev. Lett.* 117, 185301 (2016).
- [16] Y.-J. Lin, K. Jiménez-García, I. B. Spielman, *Nature* 471, 83 (2011).
- [17] D. Campbell, R. Price, A. Putra, A. Valdés-Curiel, D. Trypogeorgos, and I. B. Spielman, *Nat. Commun.* 7, 10897 (2016).
- [18] J.-R. Li, J. Lee, W. Huang, S. Burchesky, B. Shteynas, F. C. Top, A. O. Jamison, and W. Ketterle, *Nature* 543, 91 (2017)
- [19] T. Ozawa and G. Baym, *Phys. Rev. Lett.* 109, 025301 (2012)
T. Ozawa and G. Baym, *Phys. Rev. Lett.* 110, 085304 (2013)
T. Ozawa and G. Baym, *Phys. Rev. A* 85, 063623 (2012)
E. Kawasaki and M. Holzmann, *Phys. Rev. A* 95, 051601(R) (2017).
- [20] E. P. Gross, *Nuovo Cim.* 20, 454 (1961)
L.P. Pitaevskii, *Zurn. Eksp. Teor. Fiz.* 40, 646 (1961)[English Transla.: *Sov. Phys. JETP* 13, 451 (1961)].
- [21] A. Putra, F. Salces-Carcoba, Y. Yue, S. Sugawa, and I. B. Spielman, *Phys. Rev. Lett.* 124, 053605 (2020).
- [22] Y. Li, G. I. Martone, L. P. Pitaevskii, and S. Stringari, *Phys. Rev. Lett.* 110, 235302 (2013).
- [23] S. K. Adhikari, *Phys. Rev. A* 103, L011301 (2021)
S. K. Adhikari, *Phys. Lett. A* 388, 127042 (2021).
- [24] S. K. Adhikari, *J. Phys.: Consens. Matter* 33, 265402 (2021).
- [25] R. Y. Chiao, E. Garmire, and C. H. Townes, *Phys. Rev.*

- Lett. 13, 479 (1964).
- [26] Y. S. Kivshar and B. A. Malomed, *Rev. Mod. Phys.* 61, 763 (1989)
S. K. Adhikari, *Phys. Rev. A* 69, 063613 (2004).
- [27] V. Achilleos, D. J. Frantzeskakis, P. G. Kevrekidis, and D. E. Pelinovsky, *Phys. Rev. Lett.* 110, 264101 (2013).
- [28] H. Sakaguchi, B. Li, and B. A. Malomed, *Phys. Rev. E* 89, 032920 (2014)
H. Sakaguchi and B. A. Malomed, *Phys. Rev. E* 90, 062922 (2014).
- [29] Y.-C. Zhang, Z.-W. Zhou, B. A. Malomed, and H. Pu, *Phys. Rev. Lett.* 115, 253902 (2015).
- [30] S. Autti, V. V. Dmitriev, J. T. Makinen, A. A. Soldatov, G. E. Volovik, A. N. Yudin, V. V. Zavjalov, and V. B. Eltsov, *Phys. Rev. Lett.* 117, 255301 (2016).
- [31] B. Ramachandhran, B. Opanchuk, X.-J. Liu, H. Pu, P. D. Drummond, and H. Hu, *Phys. Rev. A* 85, 023606 (2012).
- [32] D. L. Campbell, G. Juzeliūnas, and I. B. Spielman, *Phys. Rev. A* 84, 025602 (2011)
B. M. Anderson, I. B. Spielman, and G. Juzeliūnas, *Phys. Rev. Lett.* 111, 125301 (2013)
Z.-F. Xu, L. You, and M. Ueda, *Phys. Rev. A* 87, 063634 (2013).
- [33] L. Salasnich, A. Parola, and L. Reatto, *Phys. Rev. A* 65, 043614 (2002)
- D. S. Petrov, M. Holzmann, and G. V. Shlyapnikov, *Phys. Rev. Lett.* 84, 2551 (2000)
M. Holzmann, M. Chevallier, and W. Krauth, *Phys. Rev. A* 81, 043622 (2010).
- [34] W. Bao and Y. Cai, *Commun. Comput. Phys.* 24, 899 (2018).
- [35] R. Ravisankar, D. Vudragović, P. Muruganandam, A. Balaž, and S. K. Adhikari, *Comput. Phys. Commun.* 259, 107657 (2021)
P. Muruganandam and S. K. Adhikari, *Comput. Phys. Commun.* 180, 1888 (2009)
D. Vudragović, I. Vidanović, A. Balaž, P. Muruganandam, S. K. Adhikari, *Comput. Phys. Commun.* 183, 2021 (2012).
P. Kaur, A. Roy and S. Gautam, *Comput. Phys. Commun.* 259, 107671 (2021)
- [36] K.-P. Marzlin, W. Zhang, and B. C. Sanders, *Phys. Rev. A* 62, 013602 (2000).
- [37] Y. V. Kartashov and D. A. Zezyulin, *Phys. Rev. Lett.* 122, 123201 (2019).
- [38] V. M. Pérez-García and J. B. Beitia, *Phys. Rev. A* 72, 033620 (2005)
S. K. Adhikari, *Phys. Lett. A* 346, 179 (2005)
S. K. Adhikari, *Phys. Rev. A* 72, 053608 (2005).